ANNALS OF GEOPHYSICS, 67, 2, SE216, 2024; doi:10.4401/ag-9094
OPEN ACCESS

Integration of Microtremor and PS-INSAR Analysis to Investigate the Susceptible Area in the Pronojiwo District (Indonesia) Following the 2021 East Java M6.1 Earthquake

Harun Arrasyid[1,2], Suwarto[1], Sukir Maryanto[*,1,2], Sri Dwi Wuryani[2], Didik R. Santoso[1], Aris Subagiyo[3]

(1) Brawijaya University, Department of Physics, Malang, Indonesia
(2) Brawijaya University, Brawijaya Volcano and Geothermal Research Center, Malang, Indonesia
(3) Brawijaya University, Urban and Regional Planning Program, Faculty of Engineering, Malang, Indonesia

Article history: received April 4, 2024; accepted June 6, 2024

Abstract

The East Java M = 6.1 Earthquake struck on April 10, 2021, at the bottom of the Indian Ocean, about 96 km south of Kepanjen District, Malang Regency, Indonesia. The neighbouring Pronojiwo District in Lumajang Regency suffered significant damages and loss of lives. The earthquake aftermath underscored the necessity of examining susceptibility factors in the Pronojiwo area for future mitigation efforts. This research focuses on assessing earthquake vulnerability in Pronojiwo District using two methodologies: microtremor analysis and PS-InSAR. Microtremor data were directly collected, while PS-InSAR data were acquired from the Sentinel-1 satellite and processed using the StamPS algorithm. Results from the microtremor analysis reveal seismic vulnerability index values ranging from 0.579×10^{-6} to 24.840×10^{-6} s^2/cm, in Pronojiwo District, with notably higher values found in areas with Semeru deposits, characterized by soft sediments. PS-InSAR analysis indicates concentrated negative shifts in residential zones, signaling structural damage. Regions with elevated vulnerability index values and negative PS points are considered more prone to earthquakes and subsequent building damages.

Keywords: Microtremor; PS-InSAR; Seismic Vulnerability Index; Pronojiwo District; Earthquake-Prone area; 2021 East Java M = 6.1 Earthquake

1. Introduction

East Java, a province located on Java Island, Indonesia, experiences a notable level of seismic activity, primarily characterized by earthquakes ranging from magnitudes of 4.8 to 5.5 on the Richter scale [Shohaya et al., 2013]. The severity of earthquake-induced damage is influenced by various factors including building strength and quality, earthquake magnitude, depth of the earthquake source, distance from the hypocenter, and duration of shaking

[Irsyam et al., 2020]. Additionally, local geological conditions significantly impact earthquake intensity. Nakamura [2000] observed that in numerous earthquakes worldwide, areas situated on alluvial plains suffer more extensive damage compared to compact hilly regions.

A relevant case study, for example, was an earthquake struck on April 10, 2021, with a magnitude of 6.1 Mw. This seismic event originated from the subduction zone, located in the Indian Ocean, south to the Java Island, Indonesia. The hypocenter was 80 km deep and 96 km south of Kepanjen district in Malang Regency, East Java. The earthquake generated ground shaking intensities ranging from II to VI on the Modified Mercalli Intensity (MMI) scale [BMKG, 2021]. The impact was profound, leading to a disaster along the southern coast of Java Island, resulting in the loss of 9 lives and injuring 121 individuals in Malang and Lumajang Regencies. Furthermore, the earthquake caused damage to 649 public facilities (Fig. 1), with 2,491 buildings severely affected, 5,038 buildings experiencing moderate damage, and 6,472 buildings sustaining minor damage [ESDM, 2021]. According to data from the Regional Disaster Management Agency (BPBD) of Lumajang Regency, Pronojiwo District was among the hardest-hit areas. Therefore, to facilitate future mitigation efforts, a vulnerability map is crucial for identifying regions susceptible to earthquakes and potential building damage.

Figure 1. Damaged building in Lumajang District after the 2021 East Java Earthquake [BPBD Lumajang, 2021].

The microtremor method is frequently used to assess the potential damage that could be caused by earthquakes due to its ability to estimate the risk level posed by seismic activity in a local geological condition. Previous studies employing microtremor analysis include research by Jamal et al. [2017], utilizing the method for microzoning of the disaster-prone areas, and by Robiana and Cipta [2021], investigating earthquake hazard potential in Bali. The Horizontal to Vertical Spectral Ratio (HVSR) analysis as one of the microtremor analysis methods, generates a curve that depicts the dynamic soil characteristics at the location of data acquisition, providing information in the form of dominant frequency (fo) and amplification factor (Ao) [Nakamura, 2000].

Ground deformations after an earthquake are very likely to occur, and remote sensing approach can be used for detecting the changes in the earth's surface. Remote sensing is a technique for collecting information about the Earth's surface from a distance using tools like satellites and aircrafts with the application in various field, such as environmental monitoring, agriculture, geology, climate studies, disaster management, urban planning, and biodiversity assessment. It involves passive (reflective) and active (emission and detection) methods to gather data needed for different analyses. The technology's ongoing improvements can provide tools for informed

decision-making and research across different domains [Yussupov and Suleimenova, 2023]. InSAR (Interferometric Synthetic Aperture Radar) analysis is a satellite data processing technique with capabilities of measuring ground movement in millimeters scale with a spatial resolution of 5-10 meters over a large area [Ferretti et al., 2007]. The advanced InSAR technique, known as PS-InSAR (Persistent Scatterer InSAR), enhances the quality of results obtained from conventional InSAR methods. PS-InSAR works by comparing various series of interferogram pairs and identifying pixels exhibiting "stable" persistent behavior [Kiseleva et al., 2014].

Although not directly employed in earthquake deformation analysis, the PS-InSAR and InSAR methods have been widely used in recent research related to deformation phenomena. There are various purposes on utilizing PS-InSAR, such as investigating the effect of groundwater level on land subsidence [Gezgin, 2022], detecting surface deformation in geothermal areas [Maghsoudi et al, 2018], characterizing earthquake swarms in India [Srijayanthi et al., 2022] and conventional InSAR research to investigate the seismic co- seismic and post- seismic deformation in the case of the 2016 Menyuan earthquake in Southwest China [Qu et al, 2021]. Both of these methods could be used to investigate susceptible areas, in order to mitigate the damage caused by earthquakes in the Pronojiwo District, Lumajang Regency. The impact of the damage can be estimated by mapping the seismic vulnerability (K_g), using the microseismic method, and the shift of ground surface deformation following an earthquake can be analyzed using remote sensing methods i.e. the PS-InSAR technique.

2. Geological Setting

Pronojiwo District composes of several formations and rock units. From the oldest, the rock formations can be sorted as follows: Mandalika Formation (Tomm), Wuni Formation (Tmw), Jembangan Volcanic Deposits (Qvj), Semeru Volcanic Deposits (Qvs), Avalanche Deposits from Nuee Ardente (Qvl), and Semeru Volcanic Deposits (Qlv), as well as swamps and rivers deposits (Qas). In addition to these rock formations, the regional geological map of

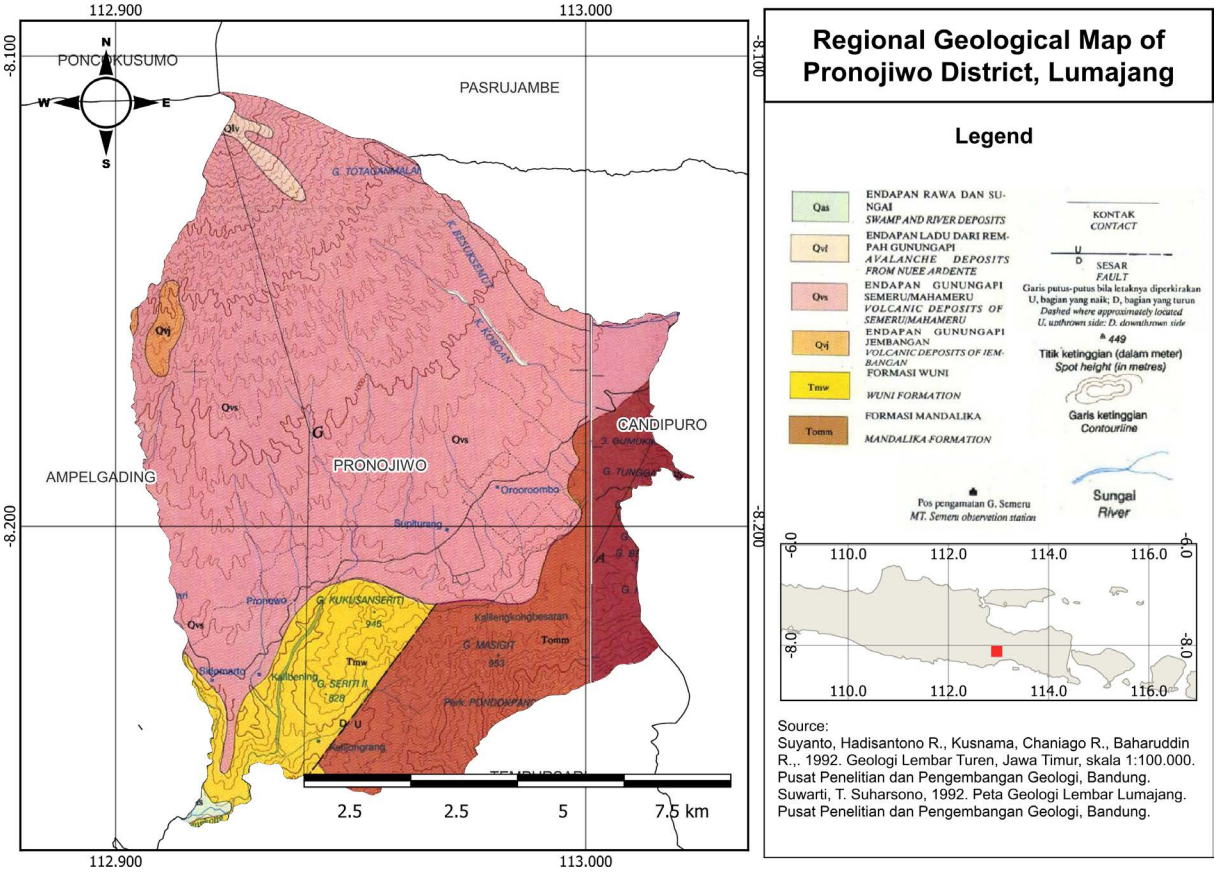

Figure 2. Regional geological map of Pronojiwo, Lumajang [Modified after Suyanto, 1992].

Pronojiwo District also indicates the presence of faults and lineaments-oriented northeast-southwest (Fig. 2). Each rock formation consists of various rocks, detailed as follows:

- **Tomm-Late Oligocene**: Mandalika Formation: andesite lava, basalt, trachyte, dacite and propylized andesite breccia.
- **Tmw-Middle Miocene**: Wuni Formation: consist of andesite-basalt breccia and lava, tuff breccia, lava breccia and sandy tuff.
- **Qvj-Early Quartenary**: Jembangan Volcanic Deposits: olivine pyroxene basalt lava, tuff, sandy tuff, sand.
- **Qvs-Middle Quartenary**: Semeru Volcano deposits: andesite lava to basalt, volcanic clastics and lava.
- **Qvl-Late Quartenary**: Avalanche Deposits from Nuee Ardente: lava deposits.
- **Qas-Late Quartenary**: Swamp and River Deposit: gravel, sand, clay and plant remain.

3. Materials and Method

This research included the microtremor measurement and analysis combined with the remote sensing by PS-InSAR analysis technique within Pronojiwo District, Lumajang Regency. Microtremor data were recorded using the Digital Portable Seismograph TDL 303-S, with a sampling rate of 100 Hz over a duration of 30-40 minutes. The data collection covered area of 8.5 km × 7.5 km with 46 acquisition points taken during the September-December 2022 time period (Fig. 3). For the PS-InSAR analysis, we utilized 8 satellite datasets in the period of March 2021 to May 2021 of the Sentinel-1 Single Look Complex (SLC) data type, the DEM, and the orbital data, obtained from ASF-Alaska Satellite Facility. One dataset was selected as the master, namely April 2021, and the remaining data served as slaves. All data were acquired from the Sentinel-1A satellite with an ascending orientation (south-north) and a wavelength of 0.56 cm, classified as C-band type and VV polarization. The data cover a resolution of 5 × 20 meters, since it is an interferometric wide swath mode [Flores et al., 2018].

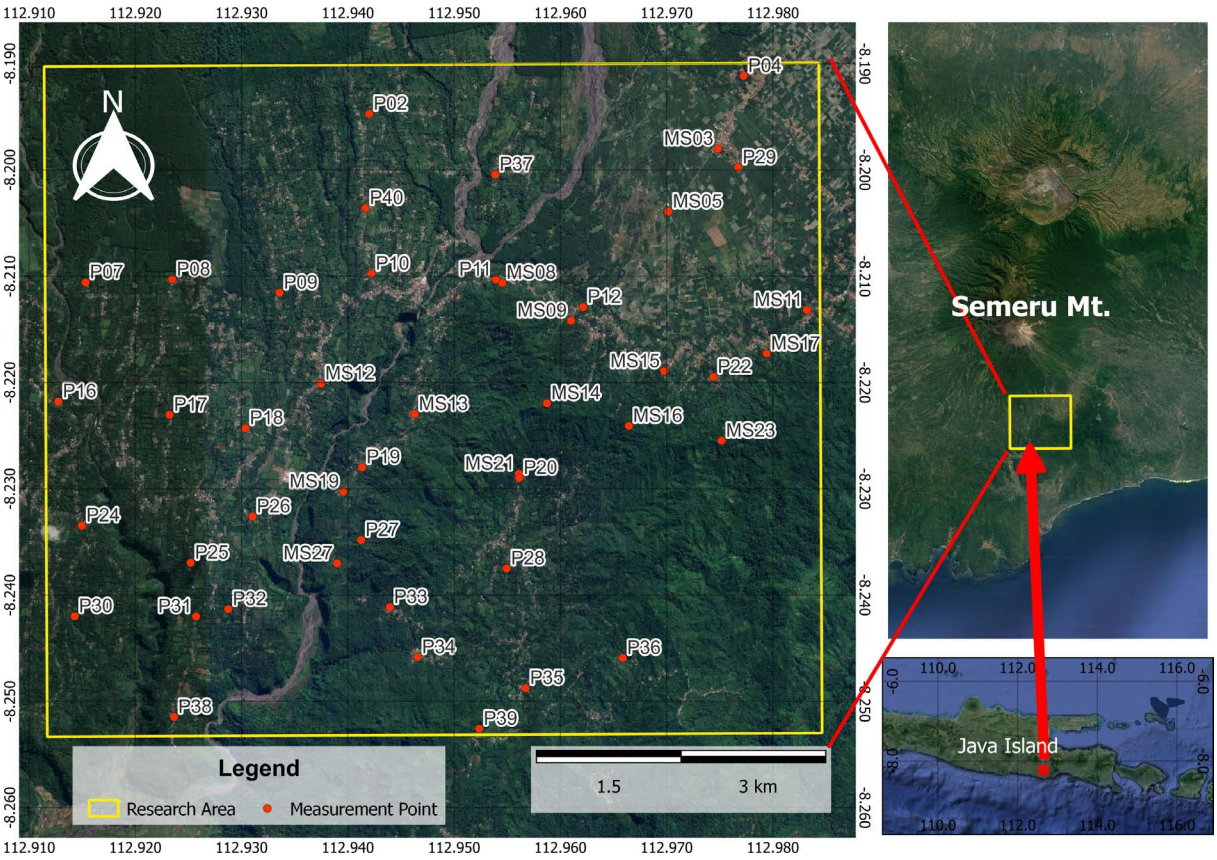

Figure 3. Review map of the research area showing the location of microtremor measurement points.

3.1 Microtremor Analysis

Microtremors are natural harmonic vibrations of soil which occur continuously. These phenomena caused by micro-vibrations below the soil surface and other natural activities, which trapped in the surface sediment layer and reflected by the presence of a boundary layer with a fixed frequency [Jamal et al., 2017]. Microtremor research allows the determination of the soil layers' characteristics based on the parameters such as dominant period and wave amplification factor.

The HVSR (Horizontal to Vertical Spectral Ratio) method is recognized as an effective, economical, and environmentally friendly technique, as well as suitable for application in residential areas. The HVSR method utilizes three-component passive seismic-measurement data i.e., microtremors. This method produces two important parameters: natural frequency (dominant frequency) and amplification factor. Both parameters are related to the subsurface physical properties, thereby useful for local geological characterization [Herak, 2008].

The determination of the seismic vulnerability index value requires attention to the shear strain on the soil surface. The magnitude of the shear strain (γ) can be calculated using the following equation [Nakamura, 1997]:

$$\gamma = \frac{A_0 \delta}{D} \tag{1}$$

where A_0 is the amplification factor, δ is the shift of the seismic wave in the bedrock (m), D is the thickness of sediment at the surface (m). The dominant frequency (f_0) at the soil surface is formulated as follows [Nakamura, 1997]:

$$f_0 = \frac{v_s}{4D} \tag{2}$$

So, the thickness of the sedimentary layer is:

$$D = \frac{v_s}{4f_0} \tag{3}$$

and the magnitude of the dominant frequency in bedrock is:

$$f_0 = \frac{v_b}{4A_0 D} \tag{4}$$

where v_s is the velocity of wave displacement on the surface, and v_b is the velocity of wave displacement on the bedrock. The wave acceleration in bedrock, α_b, can be formulated as:

$$\alpha_b = (2\pi f_0)^2 \delta \tag{5}$$

If equation (1) is formulated by including equations (4) and (5), thus obtained:

$$\gamma = \frac{A_0 \alpha_b}{(2\pi f_0)^2} \frac{4A_0 f_0}{v_b} = \frac{A_0^2}{f_0} \frac{\alpha_b}{\pi^2 v_b} \tag{6}$$

The efficiency of applying the dynamic force that affects the strain is e% of the static force, then the magnitude of the effective strain γ_e is:

$$\gamma_e = K_g(e)\alpha_b \tag{7}$$

Hence, obtained:

$$K_g = \frac{A_0^2}{f_0}\frac{1}{(\pi^2 v_b)} \tag{8}$$

The value of v_b is nearly constant in an area and K_g can be considered as an index of the susceptibility of a deformed area measured at a point K_g value on the $\times 10^{-6}$ scale (s^2/cm).

3.2 PS-InSAR Analysis

Electromagnetic waves emitted from satellites scatter when they hit certain objects on the Earth's surface. Scattering phenomenon which aimed at returning the signal back to the satellite and behaves similar to a mirror perpendicular to the direction of the incident wave, is called backscatter [Zhou et al., 2013]. Scatterers that change the distance between two datasets at different times will have a phase difference that is proportional to the time delay that occurs in the wave propagation back to the satellite. The relationship is described in equation (9) below.

$$\phi = \frac{2\pi}{\lambda} 2R = \frac{4\pi R}{\lambda} \tag{9}$$

The pair of images referred to in this method are the two focused SAR images of the master and slave. The phase difference is calculated by multiplying the master pixel by the conjugate of the slave image complex, followed by multiplying the amplitude of both master and slave images [Parker, 2017]. In addition to the surface deformation components, the interferogram phase (ϕ_{LOS}) also contains other components, namely $\Delta\phi_{geom}$. These components are related to the difference in the geometry of the satellite's view, phase difference from the topography $\Delta\phi_{topo}$, and phase difference from the atmospheric refraction $\Delta\phi_{atm}$, as described in equation (10).

$$\phi_{LOS} = \Delta\phi_{def} + \Delta\phi_{geom} + \Delta\phi_{topo} + \Delta\phi_{atm} + \phi_{error} \tag{10}$$

The geometry factor is resolved by applying the exact orbit and estimating the perpendicular baseline between orbits of satellites. This effect was eliminated by assuming ellipsoidal smooth earth. However, errors in predicting satellite orbits are arise due to solar radiation pressure. DEM (Digital Elevation Model) data was used in processing to eliminate the phases error introduced by the topography. The largest source of phase error was caused by variations in atmospheric refraction, $\Delta\phi_{atm}$, between acquisitions. ϕ_{error} represents an additional noise that describes the phase noise caused by scattering and heat noise from the instruments [Parker, 2017].

The results of co-registration and interferograms were exported for further processing using the Stanford Method for Persistent Scatterers (StaMPS) method, implemented in MATLAB software. StaMPS is a PS-InSAR processing technique that uses a set of C++-based software and MATLAB scripts regularly based on the Hooper algorithm [Hooper et al., 2012]. This method was developed to be usable even if it applied in terrain without man-made structures or irregular deformations [Hooper et al., 2018].

This study involved seven stages of StaMPS technique. The first stage was data loading, used to input the co-registration and interferogram data to the StaMPS algorithm in the required format and location. The second step was phase noise estimation by estimating the phase-noise value of each candidate pixel for each interferogram. This phase noise estimation relied on several parameters including the maximum topographical error, pixel size, weighting of each pixel, combined low-pass and adaptive phase filters, and maximum number of iterations [Hooper et al., 2012]. The third step is the PS selection process, which was selected based on the phase-noise criteria from the previous stage. In this stage, the percentage density of other (non-PS) pixels are also estimated. The fourth stage was the PS weeding stage, aimed to sorts and eliminates unselected pixels. Fifth stage was phase correction, where the phase of spatially correlated pixels was corrected. The sixth step was stamps, which converts the interferogram units $-\pi$ to π to an absolute phase integer multiplier 2π, as this is more related to topography and

deformation. The phase variation between any two points on a flattened interferogram provides a measurement of the actual height variation after removing all integers from the height [Ferretti et al., 2007]. Finally, the estimated spatially correlated look angle error stage calculates the correlated look angle error observed in stages three and five. Through all of the processing stages, a map illustrating the distribution of LOS (Line-of-Sight) measurements over time was obtained.

4. Results and Discussion

PS-InSAR processing from a master interferogram and seven slave interferograms resulted in the distribution of displacement velocity or a shift towards LOS (Line-of-Sight). In general, the shift in the study area are ranged from –25 mm/year to 48 mm/year (Fig. 4). The negative value, marked in blue colour, indicates that the point on the ground surface depicted by the PS pixel move away from the satellite LOS, or the downward movement of the ground surface. On the other hand, positive values (coloured in red) represent that point is moving closer to the satellite LOS, or upward movement of ground surface.

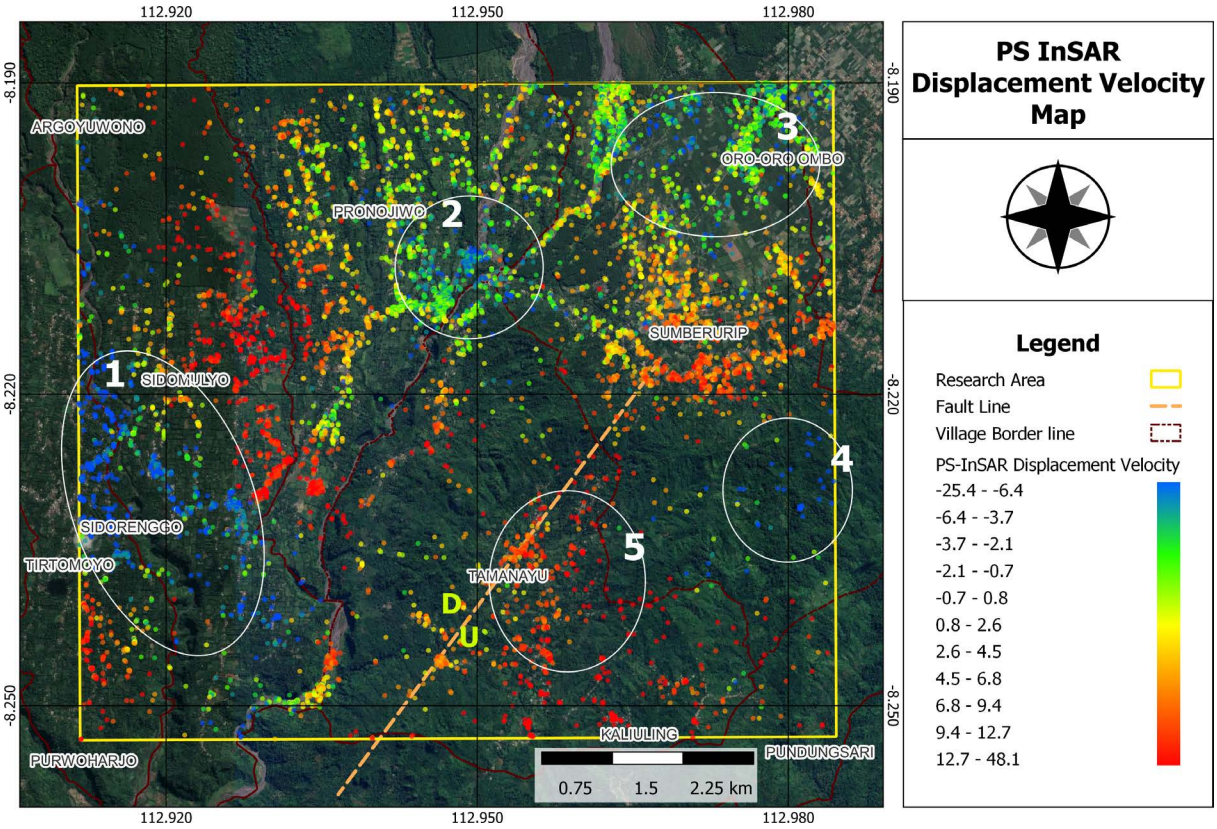

Figure 4. Map of the Pronojiwo District showing the displacement velocity pattern obtained from PS-InSAR analysis.

Changes in the land surface identified by PS-InSAR can be caused by several factors, such as: high groundwater level [Gezgin, 2022], the presence of geothermal injection wells [Maghsoudi et al. 2018], deformation due to landslides [Greif and Vlcko, 2012] or earthquake [Qu et al., 2021], deposition of pyroclastic materials after eruption [Perwita et al., 2023], or human activity [Gao et al., 2019]. Four areas with negative shift (blue dots in Fig. 4) are distributed in the central to southern parts of Sidomulyo Village, east of Pronojiwo Village, and north and south of Sumberurip Village. These areas of negative shift are mostly located within residential zones, indicating potential damage to houses resulting from the earthquake that occurred on April 10, 2021. The interpretation of the PS-InSAR aligns with the data of substantial damage of houses in the Pronojiwo District (Table 1), including the Pronojiwo village, Sidomulyo village, and Tamanayu village as presented by the BPBD Lumajang [BPBD Lumajang, 2021].

No	District	Village	Total
1	Candipuro	Penanggal Sumbermujur Sumberwuluh	13 1 2
2	Gucialit	Kertowono Pakel Tunjung	37 4 2
3	Jatiroto	Banyuputih Kidul	1
4	Kedungjajang	Sawaran Kulon	4
5	Pasirian	Bades Condro	7 2
6	Pasrujambe	Jambearum Jambekumbu Karanganom Kertosari Pagowan Pasrujambe	8 15 1 4 1 219
7	Pronojiwo	Oro-Oro Ombo Pronojiwo Sidomulyo Sumberurip Supiturang Tamanayu	92 279 469 23 58 426
8	Senduro	Argosari Burno Kandangan Kandang Tepus Ranupani Senduro Wono Cempoko Ayu	34 6 3 2 1 20 4
9	Sumbersuko	Sentul	1
10	Tekung	Tukum	1
11	Tempursari	Kaliuling Pundungsari Purorejo Tempursari	817 80 18 32
12	Yosowilangun	Karangrejo Kebonsari	1 1
		Total	**2687**

Table 1. The number of houses damaged in the East Java Earthquake in April 2021, sorted by district and village in the Lumajang Regency [BPBD Lumajang, 2021].

However, these results cannot fully describe the occurrence of damage in Tamanayu Village, as positive values on PS-InSAR are observed.

The positive anomaly in Tamanayu Village is possibly caused by the reactivation of the fault, marked by the dotted line on the regional geological map of Pronojiwo (Fig. 2). Based on Geology Map [Suyanto et al., 1992], the fault that passes through Tamanayu Village is categorized as dip-slip fault, with the eastern part of the block moving upward (denoted by the letter U on the map). Reactivation of such of fault type can occur when external forces traverse the fault. For example, in the case of the Bantul earthquake in May 2006, the severely damaged area was associated with an old fault area possibly experiencing fault reactivation [Blanco-Martín et al., 2022]. Following the earthquake on April 10, 2021, the area in the east of Tamanayu Village was moving up compared to the area in the west, and this caused the positive value of the vertical shift at point PS (illustrated in orange-red colour, Fig. 4) although, in reality, there was a lot of damaged houses in the area.

By using the horizontal to vertical ratio formula, the H/V value is obtained as shown in Fig. 5. The H/V (Horizontal to Vertical Spectral Ratio) curve obtained from 46 microtremor measurement points in the study area generate two outputs: (1) the dominant frequency (the horizontal axis of the peak of the H/V curve, Fig. 5), and (2) the amplification factor (the vertical axis of the peak of the H/V curve, Fig. 5). For each measurement point, the spectrum was also calculated, and the trend for each component were showing similarity to the spectrum at MS08, as shown in Fig. 6. Seismic vulnerability index was calculated from these two values. The dominant frequency, amplification factors, and seismic vulnerability index are beneficial for monitoring the area's vulnerability to earthquakes. In addition, there is a qualitatively positive correlation between the response of HVSR curve and the extent of damage that occurred around the fault, as resulted by the previous research on the Bantul earthquake in May 2006 [Daryono and Prayitno, 2009].

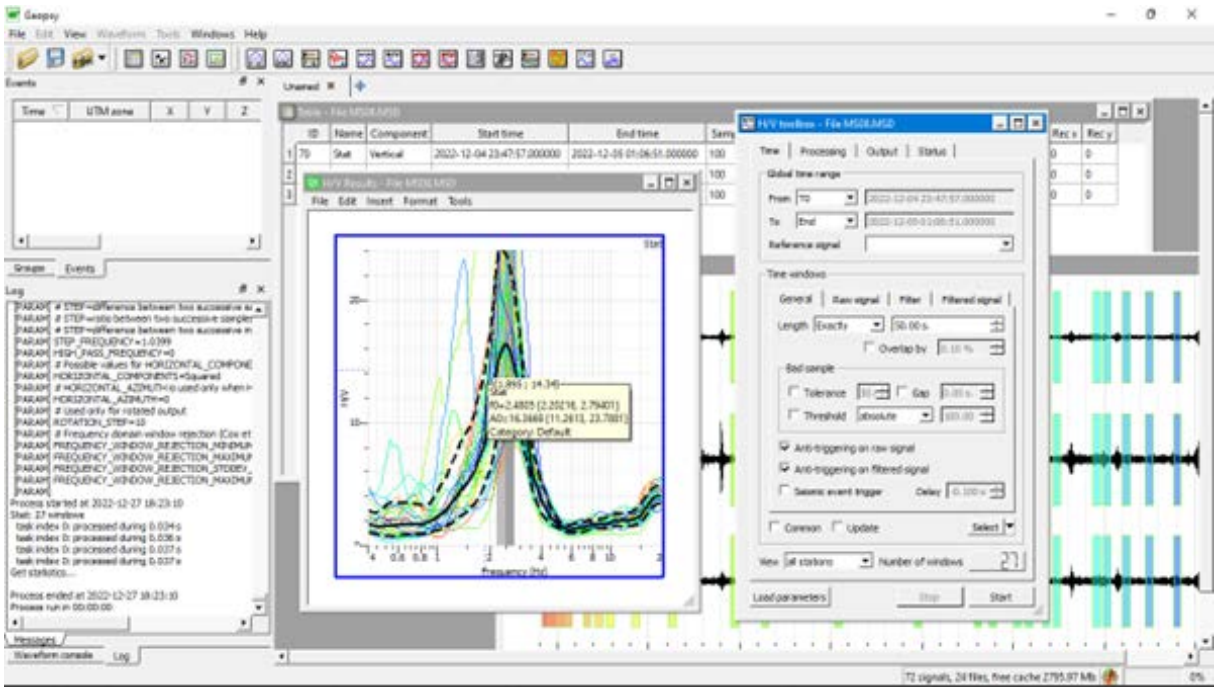

Figure 5. Analysis of the measurement point MS08 showing the H/V curve and f_0 and A_0 values, using Geopsy Software.

The distribution of dominant frequency values, f_0 of the research area is illustrated in Fig. 7. The dominant frequency values are ranged from 0.579 Hz to 11.481 Hz, with low f_0 values concentrated in the central part of Sidomulyo Village, south of Pronojiwo Village, and the central part of Sumberurip Village. Meanwhile, higher f_0 values were observed in southern and northern region. Toward the north, relatively higher f_0 values were found in the northern parts of the Sidomulyo Village, Pronojiwo Village, and Sumberurip Village. Toward the south, relatively higher, f_0 values were found in the entire Tamanayu Village, as well as in the southern part of Sidomulyo, and Sumberurip Villages.

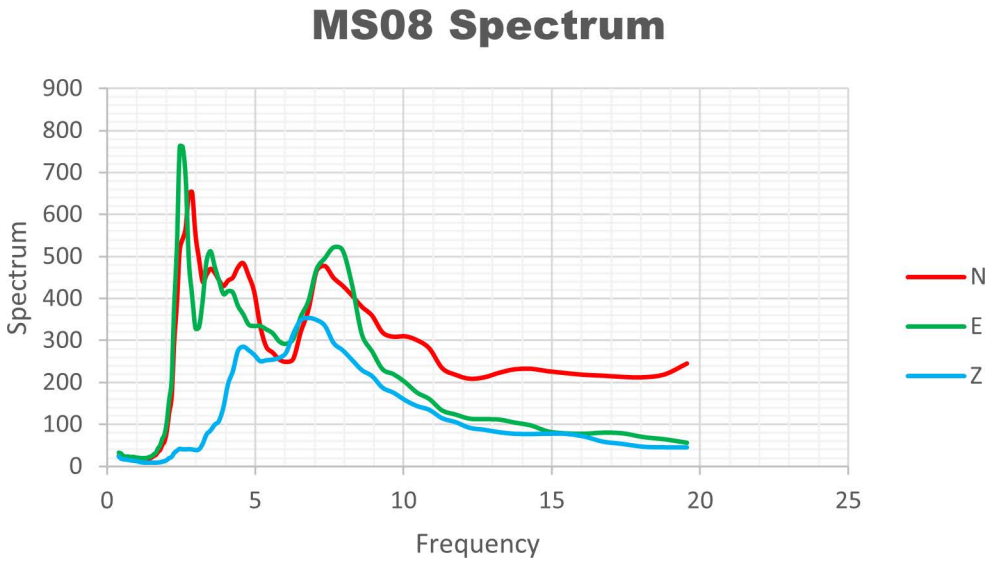

Figure 6. The spectrum of N-, E- and Z-component of seismic data at point MS08.

The dominant frequency value, f_0, also known as the natural frequency, can be an indication of the lithology and thickness of the sediment at that location [Nakamura et al., 1989]. Areas with low-frequency values (illustrated in blueish-purple, Fig. 7) mostly correspond to the Qvs formation, Semeru Volcano deposits comprising andesitic to basaltic lava, volcanic clasts, and lava [Suyanto et al., 1992]. The northern part of Qvs, with a relatively higher frequency, is interpreted to be a lithology composed of hard rocks such as andesitic lava to basalt. The southern

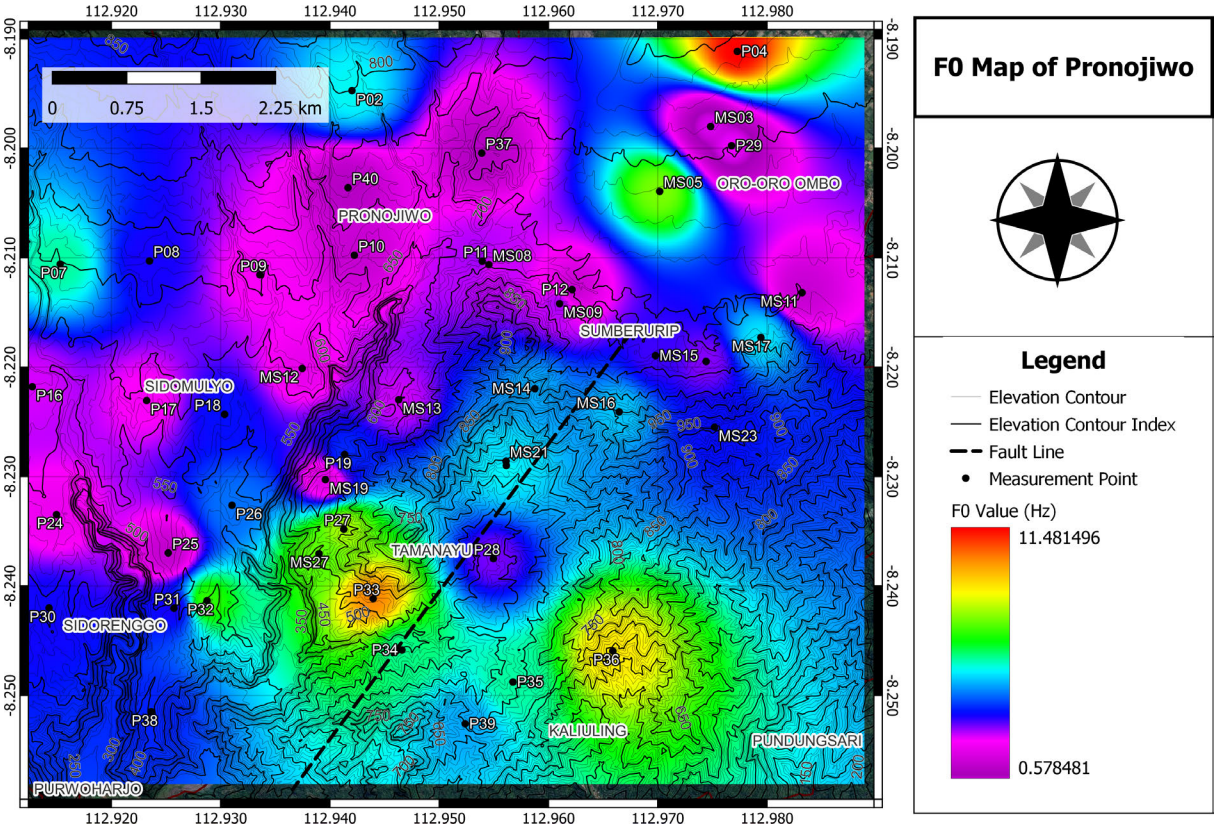

Figure 7. Map of the Pronojiwo District, showing the distribution of dominant frequencies, f_0.

part of Qvs, which has lower natural frequency, is interpreted as the area covered with volcanic clastic with thick uncompacted sediments. Present of soft lithology can increase the risk of damage in an area because of the material's tendency to provide a long-period vibration response. This effect is called site effect or site amplification [Sunardi et al., 2012].

Areas with higher elevations or hills tend to have higher natural frequencies [Nakamura, 2000], as exhibited within the research area from Tamanayu Village to the southern part of Sumberurip Village. Located between hills with high-frequency values, the areas around point P28 show relatively low-frequency recorded values. Such anomalies, can be explained with the geology of the area described in the geological map, likely resulted by the presence of local geological structure in the form of a fault. Other anomalies were also observed in the area around points MS23 and P22 in the centre of Sumberurip Village. This area shows relatively low natural frequency despite being situated in highlands and are likely composed of a different lithology with softer, lower density rocks, compared to the surrounding area. However, a further geological study is necessary to ascertain the local lithology's formation, and structures.

The H/V curve also generates the amplification factor (A_0). As illustrated in Fig. 8, the amplification factors value varying from high to very high are distributed in the southern part of Sidomulyo Village, Pronojiwo Village, the northern part of Tamanayu Village, and in the middle to southern part of Sumberurip Village. Moderate to low amplification factor values are distributed in the northern part of Sidomulyo Village, southern part of Tamanayu Village, and northern part of Sumberurip Village. The minimum value of the amplification factor in the study area is 2.786, whereas the maximum value is 18.276.

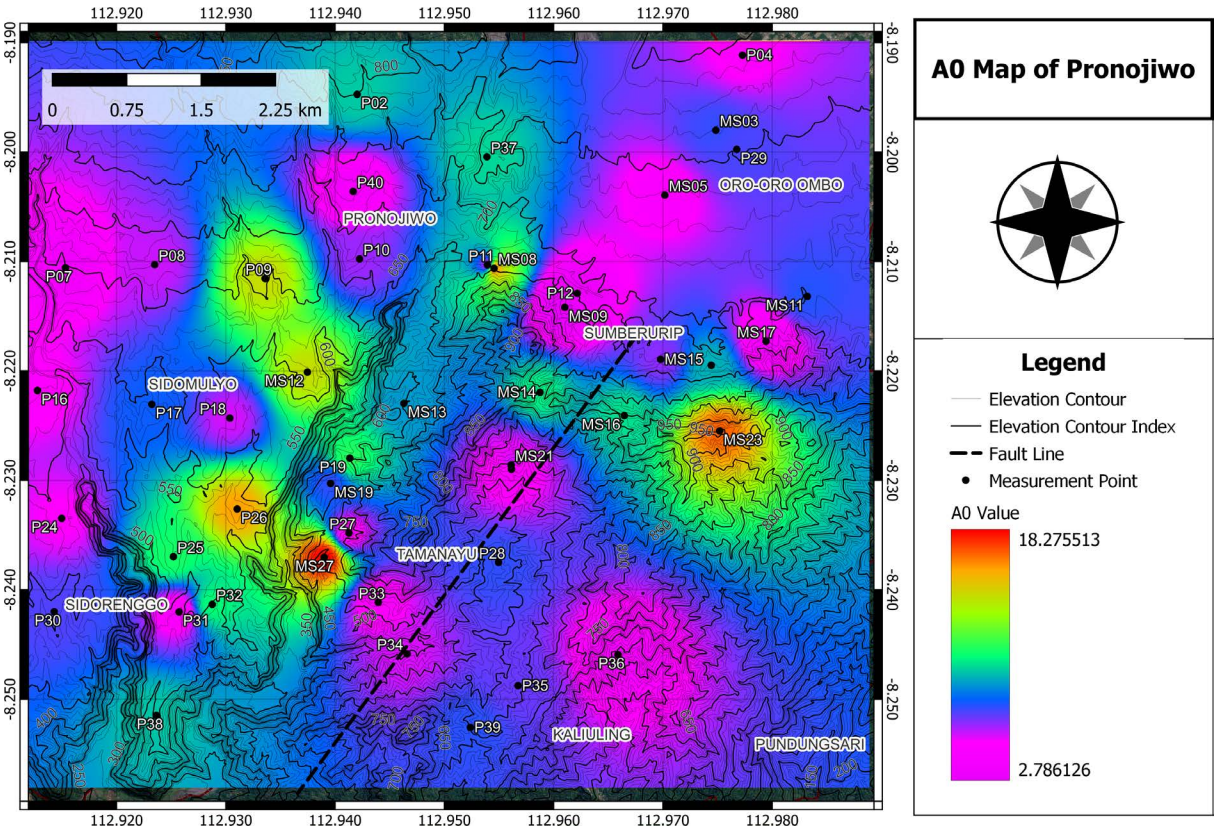

Figure 8. Map of Pronojiwo District, showing the distribution of Amplification Factors, A_0.

The amplification factor indicates the impedance ratio between the sediment layer to the bedrock. In addition, the amplification value describes the change of acceleration value of ground wave vibrations due to shear wave velocities difference between bedrock and surface sediments. When seismic waves propagate on sediments with

softer composition than the soil they traverse previously, the waves will experience amplification. The greater the difference of shear wave velocities, the greater the amplification occurred to the seismic wave [Haeruddin et al., 2019].

In the western area of Tamanayu Village, precisely at points MS27, P26, MS19, P19, MS13, MS12, and P09, high A_0 values are associated with valleys/rivers. The high amplification factors at this location are probably influenced by the sediment cover in the area around the river. Soft sediment on top of hard rock will have the magnification effect on seismic waves. Furthermore, areas with high amplification factor are also observed in the northern part of the study area, which are labelled as the Qvs formation in the geological map. This formation is predominantly composed of uncompacted pyroclastic rocks, proving that the build-up of thick pyroclastic sediments on top of hard rock can amplify seismic waves. However, anomaly that is not in accordance with the theory was again found in the area around point MS23 and P22, where these areas are included in the highlands exhibit a high amplification factor response. It is possible that the rocks in this area experienced significant weathering in their past. However, further geological studies are required to confirm this hypothesis.

The results of microtremor analysis using the HVSR method in the study area yielded seismic vulnerability index values ranging from 0.579×10^{-6} to 24.840×10^{-6} s^2/cm. The distribution of these values is illustrated in Fig. 9. The seismic vulnerability index in map represents areas with the potential to experience strong shocks in the events of an earthquake. The study areas with K_g values of below 8×10^{-6} s^2/cm (coloured in purple to dark blue) are scattered in the northern Sidomulyo Village, southern Tamanayu Village, and the central part of Sumberurip Village. Most of these low K_g values are located within the Mandalika and Wuni Formations, which are composed of hard-rock lithology.

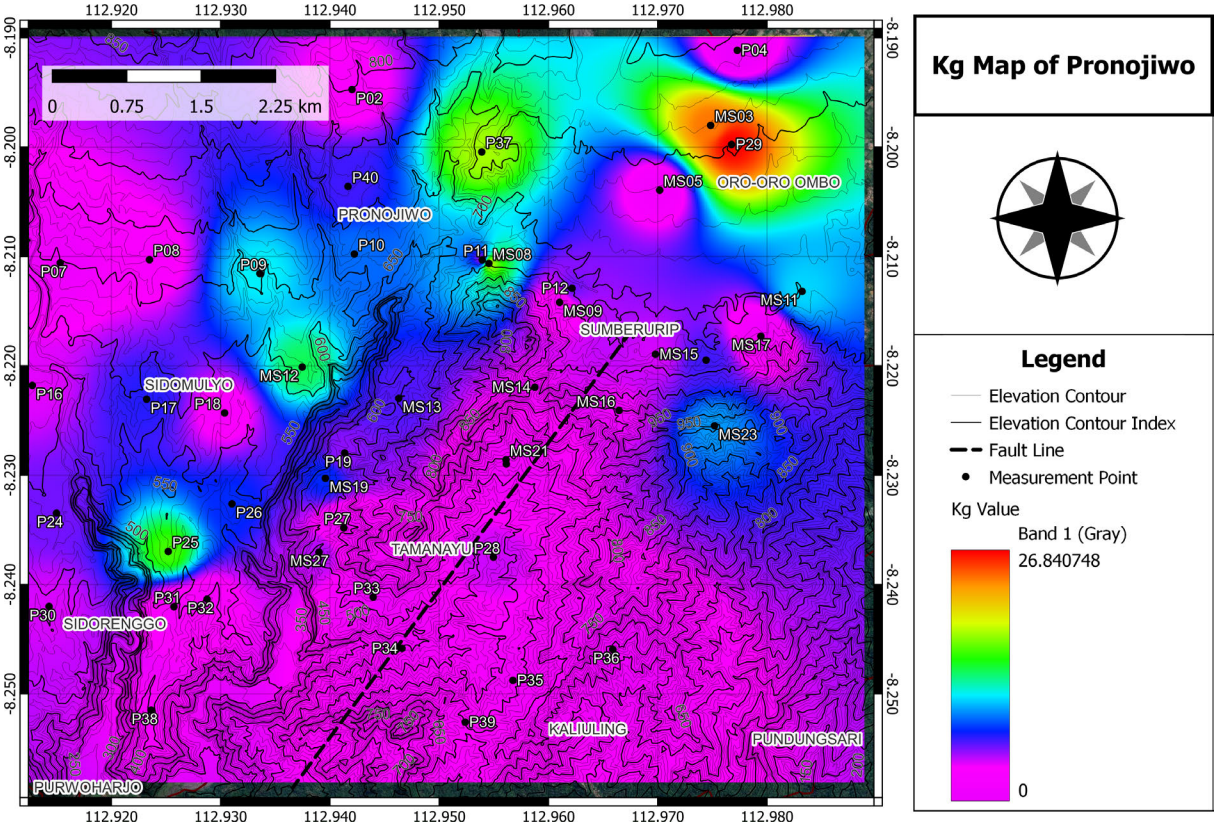

Figure 9. Map of Pronojiwo District, showing seismic Vulnerability Index (K_g) of the researched area.

In some locations, relatively high values are observed, with K_g values varying from 10×10^{-6} s^2/cm (green) to 26×10^{-6} s^2/cm (red). High K_g values are observed in the southern part of Sidomulyo Village, the central to the southern part of Pronojiwo Village, and the northern part of Sumberurip Village. Most of the areas with high K_g values are located within the Qvs Formation, corresponding to volcanic clastics. Areas with high K_g values are

prone to strong shaking when earthquake strikes because the earthquake waves experience amplification when they reach these materials. The shaking is therefore stronger, so the damage will be potentially more severe compared to areas with lower K_g values.

The microtremor results have also been interpreted together with the information on the distribution of PS-InSAR LOS displacement points, as shown in Fig. 10. On a closer observation, the distribution of points with negative values (green to blue) correlates with areas which exhibit high values of seismic vulnerability index. This correlation suggest that such areas pose high risk of damage caused by earthquakes.

Areas with high K_g values and negative PS points in this study are distributed in the southern part of Sidomulyo Village, Pronojiwo Village, and in the northern and southern parts of Sumberurip Village. Consequently, these areas are particularly vulnerable to the damage from earthquakes. Most of these vulnerable areas are located on top of clastic deposits (softer part) of the Qvs formation, and also exhibit low dominant frequency and high amplification factor. As the result, a resonance will occur when an earthquake with a wave frequency similar to the natural frequency value of the soil strikes the area. The waves passing through the area it will be amplified, potentially leading to the collapse of buildings that do not adhere to earthquake-resistant standards. Such events are represented as a negative displacement LOS value in the PS-InSAR analysis.

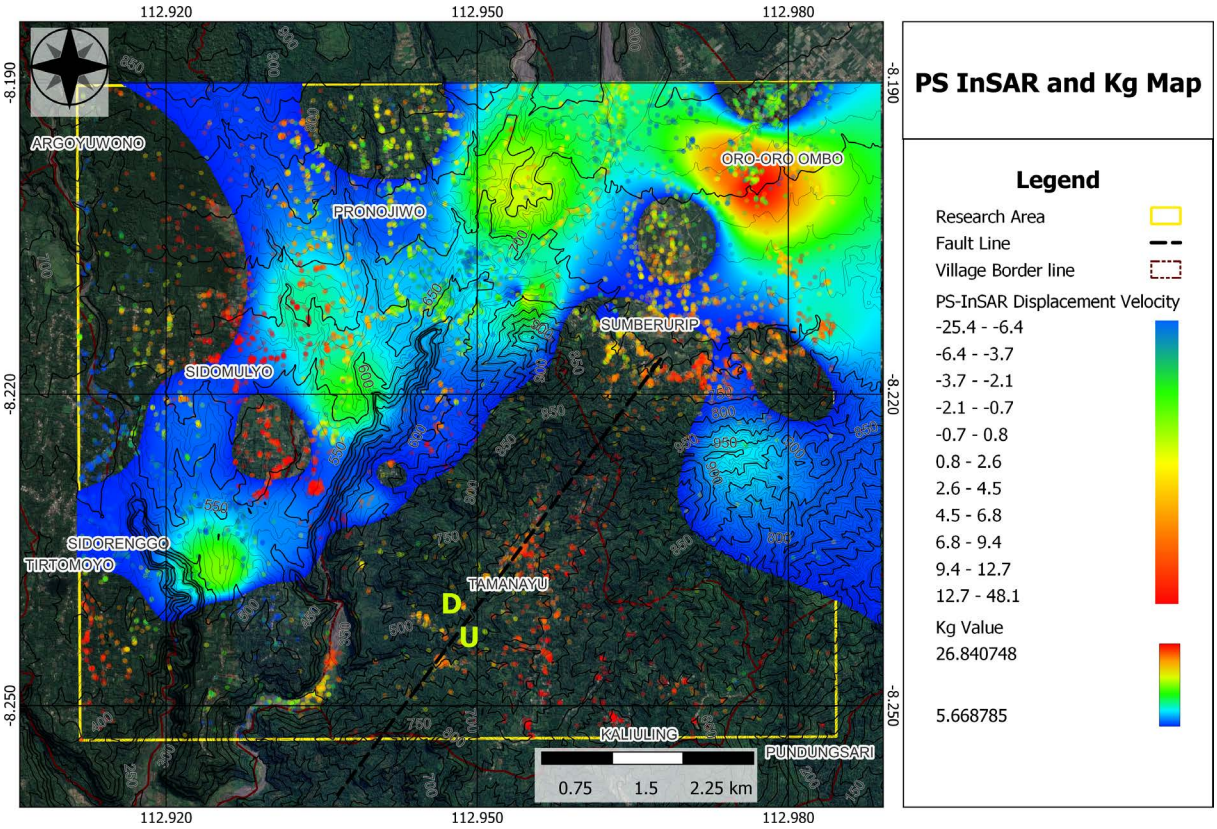

Figure 10. Map of the Pronojiwo District, showing the displacement Velocity from PS-INSAR analysis overlayed with K_g map from microseismic analysis.

Previous research conducted by Susilo et al. [2023] which covered smaller area than the location of our study (Fig. 11), supports the finding of this study, particularly in areas dominated by unconsolidated sedimentary material, as well as in hilly areas where weathering may occur. Susilo's research revealed the frequency range of approximately 1.8-6.8 Hz in the Tmw rock formation. For comparison, the range of frequency values obtained in the southwest and south of our research area is in the range from 0.57-11.48. Similarly, Susilo's research reported the amplification factor value ranging from 2.8-7, whereas the results of this study show a broader range, in around 2.78-18.27. Additionally, the K_g values obtained are also not too different. Susilo's research obtained K_g in the range of 2-19, while our research resulted values in the range of 0.57-26.8.

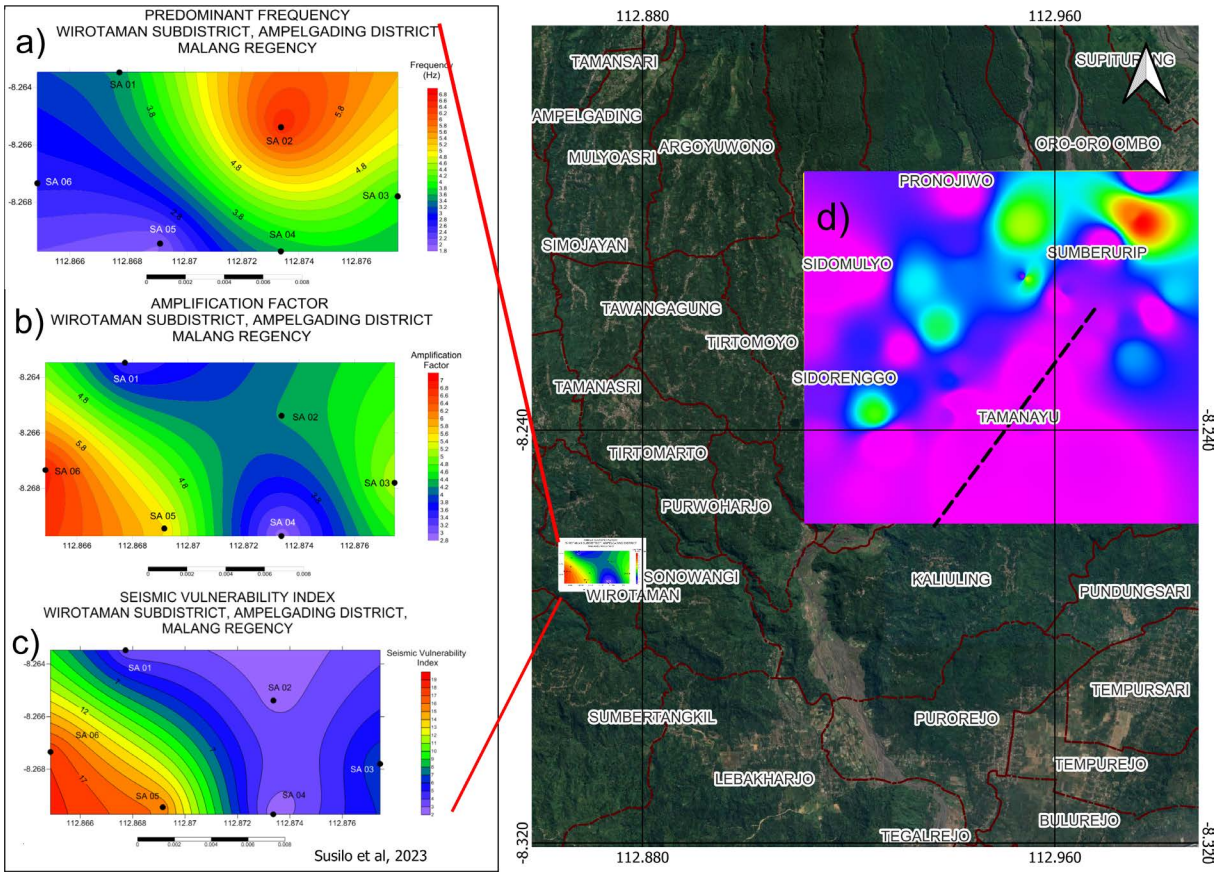

Figure 11. Correlation of the results with the previous study conducted by Susilo et al. [2023], showing Dominant Frequency-f_0 (a), Amplification factor-A_0 (b), and seismic vulnerability index-K_g (c and d).

5. Conclusion

The finding of the Microtremor analysis in Pronijiwo District show seismic vulnerability index values in the range of 0.579×10^{-6} to 24.840×10^{-6} s^2/cm. The PS-InSAR interpretation, supported by the data obtained from BPBD Lumajang, collected following the earthquake on the April 10, 2021, showed that the distribution of negative shift areas corresponds with residential areas in Pronojiwo, Sidomulyo, and Tamanayu Villages, Pronojiwo District, where majority of houses were damaged.

Most of the high seismic vulnerability index values measurement ponits were observed within Semeru deposits (Qvs formation), composed of soft volcanic clastics, and most of the vulnerable areas with high K_g values and negative PS points were located on top of the same deposits. These areas are particularly prone to earthquake-induced shocks and damages are easily possible to occur.

Earthquake hazard mapping based on microtremor and PS-InSAR is valuable reference for building design within the study area. Residents and buildings located in vulnerable areas can prioritize constructing better-quality buildings, which are more resistant to earthquakes. Furthermore, implementation of a better preventive measure, such as avoiding the development in areas with high seismic vulnerability index values will contribute in enhancing community resilience to earthquakes.

Data availability statement. Satellite data used in this study is an open access data type, obtained from The Alaska Satellite Facility (ASF), which is part of the Geophysical Institute of the University of Alaska Fairbanks at https://vertex.daac.asf.alaska.edu/. The microseismic data that support the findings of this study were acquired by the Meteorological, Climatological, and Geophysical Agency of Indonesia (BMKG), in which all access and availability of the data can only be obtained through formal correspondence directly to the agency.

Acknowledgements. This work is part of a research project Grants for Professor's Research of Faculty of Mathematics and Natural Sciences, Brawijaya University Malang under contract number: 4158.10/UN10.F09/PN/2023 and 3084.2/UN10.F09/PN/2022; Workshop of Geophysics by Geophysical Engineering Study Program, Brawijaya University Malang batch 2019; Department of Physics, Brawijaya University; and BMKG (Meteorology, Climatology and Geophysics Agency) Pasuruan especially for the microseismic data.

References

Blanco-Martín, L., E. Jahangir, A.P. Rinaldi and J. Rutqvist (2022). Evaluation of possible reactivation of undetected faults during CO_2 injection, Int. J. Greenhouse Gas Control, 121, 103794, https://doi.org/10.1016/j.ijggc.2022.103794.

BMKG (2021). Ulasan Guncangan Gempa Jatim 10 April 2021 (in English: Review of the East Java earthquake shock 10 April 2021) [online]. Retrieved from https://www.bmkg.go.id/berita/?p=ulasan-guncangan-tanah-akibat-gempabumi-barat-daya-malang-jawa-timur-10-april-2021andlang=IDands=detil, accessed 25 July 2023, (in Indonesian).

BPBD Lumajang (2021). Data Rumah Rusak Gempa Lumajang 2021 (in English: Data on Houses Damaged by Lumajang Earthquake in 2021), Unpublished database by BPBD Lumajang, (in Indonesian).

Daryono, S.Si. and B.S. Prayitno, (2009). Data Mikrotremor dan Pemanfaatannya untuk Pengkajian Bahaya Gempabumi (in English: Microtremor Data and Its Use for Earthquake Hazard Assessment), BMKG, Yogyakarta (in Indonesian).

ESDM (2021). Laporan Singkat dan Rekomendasi Teknis Gempa Bumi Jawa Timur Selatan Tanggal 10 April 2021 (in English: Brief Report and Technical Recommendations for The South East Java Earthquake on April 10 2021) [online], Retrieved from https://vsi.esdm.go.id/index.php/gempabumi-a-tsunami/laporan-singkat-dan-rekomendasi-teknis/3593-laporan-singkat-dan-rekomendasi-teknis-gempa-bumi-jawa-timur-selatan-tanggal-10-april-2021, accessed 25 July 2023, (in Indonesian).

Ferretti, A., A. Monti-Guarnieri, C. Prati, and F. Rocca (2007). InSAR Principles: Guidelines for SAR Interferometry Processing and Interpretation (TM-19, February 2007), European Space Agency, Noordwijk, Netherlands.

Flores, A.I.A., K.E. Herndon, R.B. Thapa and E. Cherrington (2018). THE SAR HANDBOOK: Comprehensive Methodologies for Forest Monitoring and Biomass Estimation, National Space Science and Technology Center, Alabama, United States, https://doi.org/10.25966/nr2c-s697.

Gao, M., H. Gong, X. Li, B. Chen, C. Zhou, M. Shi, L. Guo, Z. Chen, Z. Ni and G. Duan (2019). Land subsidence and ground fissures in Beijing Capital International Airport (BCIA): Evidence from Quasi-PS InSAR analysis, Remote Sens., 11, 12, 1466, https://doi.org/10.3390/rs11121466.

Gezgin, C. (2022). The influence of groundwater levels on land subsidence in Karaman (Turkey) using the PS-InSAR technique, Advances in Space Research, 70, 11, 3568-3581, https://doi.org/10.1016/j.asr.2022.08.003.

Greif, V. and J. Vlcko (2012). Monitoring of post-failure landslide deformation by the PS-InSAR technique at Lubietova in Central Slovakia, Environ. Earth Sci., 66, 6, 1585-1595, https://doi.org/10.1007/s12665-011-0951-x.

Haeruddin, N., F. Alami and Rustadi (2019). Mikroseismik, Mikrotremor, dan Microearthquake dalam Ilmu Kebumian (in English: Microseismics, Microtremors, and Microearthquakes in Earth Science), Pusaka Media, Lampung, Indonesia, (in Indonesian).

Herak, M. (2008). ModelHVSR-A Matlab® tool to model horizontal to vertical spectral ratio of ambient noise, Comput. Geosci., 34, 11, 1514-1526, https://doi.org/10.1016/j.cageo.2007.07.009.

Hooper, A., D. Bekaert, E. Hussain and K. Spaans (2018). StaMPS/MTI Manual Version 4.1b, University of Leeds, Leeds, UK.

Hooper, A., D. Bekaert, K. Spaans, and M. Arikan (2012). Recent advances in SAR interferometry time series analysis for measuring crustal deformation, Tectonophysics, 514-517, January 2012, 1-13, https://doi.org/10.1016/j.tecto.2011.10.013.

Irsyam, M., P.R. Cummins, M. Asrurifak, L. Faizal, D.H. Natawidjaja, S. Widiyantoro, I. Meilano, W. Triyoso, A. Rudiyanto, S. Hidayati, M. Ridwan, N.R. Hanifa and A.J. Syahbana (2020). Development of the 2017 National seismic hazard maps of Indonesia, Earthq. Spectra, 36, 1 suppl., 112-136, https://doi.org/10.1177/8755293020951206.

Jamal, J. R., S. Aswad and C. Sulaiman (2017). Mikrozonasi kawasan rawan bencana gempabumi dengan studi Peak Ground Acceleration menggunakan metode Boore Atkinson dan data mikrotremor di Daerah Kupang (in English: Microzonation of Earthquake-Prone Areas with Peak Ground Acceleration Studies Using the Boore Atkinson Method and Microtremor Data in the Kupang Region), Journal Geocelebes, 1, 1, 5-12, https://doi.org/10.20956/geocelebes.v1i1.1774.

Kiseleva, E., V. Mikhailov, E. Smolyaninova, P. Dmitriev, V. Golubev, E. Timoshkina, A. Hooper, S. Samiei-Esfahany and R. Hanssen (2014). PS-InSAR Monitoring of Landslide Activity in the Black Sea Coast of the Caucasus, Proc. Technol., 16, 2014, 404-413, https://doi.org/10.1016/j.protcy.2014.10.106.

Maghsoudi, Y., F. van der Meer, C. Hecker, D. Perissin and A. Saepuloh (2018). Using PS-InSAR to detect surface deformation in geothermal areas of West Java in Indonesia, Int. J. Appl. Earth Obs. Geoinf., 64, February 2018, 386-396, https://doi.org/10.1016/j.jag.2017.04.001.

Nakamura, Y. (1997). Seismic vulnerability indices for ground and structures using microtremor, World Congress on Railway Research, Florence, Italy, November 1997, 1-7.

Nakamura, Y. (2000). Clear identification of fundamental idea of Nakamura's technique and its applications, The 12th World Conference on Earthquake Engineering, Auckland, New Zealand, 30 January-4 February 2000, Paper No. 2656, 8 p.

Nakamura, Y., T. Sato and M. Nishinaga (2000). Local site effect of Kobe based on microtremor measurement, Proceeding of the Sixth International Conference on Seismic Zonation EERI, November 12-15, 2000, Palm Springs, California.

Nakamura, Y. (1989). A Method for Dynamic Characteristics Estimation of Subsurface using Microtremor on the Ground Surface, Quarterly Report of RTRI, Railway Technical Research RTRI, 30, 1.

Parker, A.L. (2017). InSAR Observations of Ground Deformation: Application to the Cascades Volcanic Arc, Springer Cham, UK, https://doi.org/10.1007/978-3-319-39034-5.

Perwita, C.A., F. Aprilia, S. Maryanto, H. Arrasyid and A.F. Tsabitah (2023). Hazards mitigation of lahar flows on Semeru Volcano after the 4 December 2021 Eruption based on PS-InSAR, Int. J. Disaster Med., 5, 3, 193-202, https://doi.org/10.24815/ijdm.v5i3.29098.

Qu, W., B. Liu, Q. Zhang, Y. Gao, H. Chen, Q. Wang and M. Hao (2021). Sentinel-1 InSAR observations of co- and post-seismic deformation mechanisms of the 2016 Mw 5.9 Menyuan Earthquake, North western China, Adv. in Space Res., 68, 3, 1301-1317, https://doi.org/10.1016/j.asr.2021.03.016.

Robiana, R. and A. Cipta (2021). Earthquake hazard potential based on site class condition at Amlapura Area, Karangasem, Bali, Journal of Environment and Geological Hazards, 12, 3, 159-169, http://jlbg.geologi.esdm.go.id/index.php/jlbg.

Shohaya, J.N., U. Chasanah, A. Mutiarani, L. Wahyuni and M. Madlazim (2013). Survey dan analisis seismisitas Wilayah Jawa Timur berdasarkan data gempa bumi periode 1999-2013 sebagai upaya mitigasi bencana gempa bumi (In English: Survey and analysis on the seismicity at the East Java Region based on earthquake data for the period of 1999-2013 as earthquake disaster mitigation effort), Jurnal Penelitian Fisika Dan Aplikasinya, JPFA, 3, 2, 18-27, https://doi.org/10.26740/jpfa.v3n2.p18-27.

Srijayanthi, G., R.S. Chatterjee, C. Kamra, M. Chauhan, S. Chopra, S. Kumar, P. Chauhan, H. Limbachiya and P.K. Champati Ray (2022). Seismological and InSAR based investigations to characterise earthquake swarms in Jamnagar, Gujarat, India – An active intraplate region, J. Asian Earth Sci., X, 8, December 2022, 100118, https://doi.org/10.1016/j.jaesx.2022.100118.

Sunardi, B., J. Arifin and P. Susilanto (2012). Kajian potensi bahaya gempabumi Daerah Sumbawa berdasarkan efek tapak lokal (In English: Earthquake Hazard Potential Study in Sumbawa Based Local Site Effect), Jurnal Meteorologi Dan Geofisika, 13, 2, 131-137, https://doi.org/10.31172/jmg.v13i2.127.

Susilo, A., A.M. Juwono, F. Aprilia, F. Hisyam, S. Rohmah and M.F.R. Hasan (2023). Subsurface analysis using microtremor and resistivity to determine soil vulnerability and discovery of new local fault, Civ. Eng. J., 9, 9, 2286-2299, https://doi.org/10.28991/CEJ-2023-09-09-014.

Suyanto, R. Hadisantono, Kusnama, R. Chaniago and R. Baharuddin (1992). Peta geologi lembar Turen Jawa skala 1: 100.000 (in English: Geologic map of the Turen quadrangle, Jawa on a scale 1:100.000), Geological Research and Development Centre, Bandung, Indonesia.

Yussupov, A. and R.Z. Suleimenova (2023). Use of remote sensing data for environmental monitoring of desertification, Evergreen, 10, 1, 300-307, https://doi.org/10.5109/6781080.

Zhou, Z. (2013). The applications of InSAR time series analysis for monitoring long-term surface change in peatlands, PhD thesis, University of Glasgow.

***CORRESPONDING AUTHOR: Sukir MARYANTO**,
Physics Department, Brawijaya University, Jl. Veteran No. 1 Malang, East Java, Indonesia
e-mail: sukir@ub.ac.id